Radiation and Turbulence in the Stable Boundary Layer

John M. Edwards

Met Office, FitzRoy Road, Exeter
EX1 3PB, United Kingdom
john.m.edwards@metoffice.gov.uk

1 Introduction

The representation of the stable boundary layer (SBL) in numerical forecasting and climate models is widely recognised to be problematic (Cuxart et al. (2006)). Although research on the SBL has traditionally been focused on the role of turbulence, it is becoming increasingly apparent that whilst turbulent processes are important in the SBL, the problem is not one of turbulence alone. Equal attention must be given to the coupling of the boundary layer and the land surface and to radiative processes.

Radiation plays two roles in the SBL, the principal one being in the surface flux budget, but longwave (LW) radiative cooling of the atmosphere cannot be neglected, and research on both these aspects of the problem stretches over several decades. Brunt (1941) used simple empirical relationships for the downward LW flux to discuss its role in the nocturnal surface flux budget. Measurements of radiative cooling rates in the SBL were made in the 1950s and 1960s (*e.g.* Funk (1960)), which indicated that atmospheric radiative cooling could be significant, and attempts were made to compare these measurements with the predictions of the developing radiation schemes of the period. However, a full understanding of the role of radiation was not reached.

The development of turbulence models in the 1970s led to theoretical studies of radiation and turbulence. Garratt and Brost (1981) used a single-band radiation scheme in combination with a second-order turbulence closure to investigate the impact of radiation throughout the SBL and noted the importance of radiative processes towards its top. Tjemkes and Duynkerke (1989) followed this with a study using a more sophisticated radiation scheme and found a deepening of the SBL by 25% when atmospheric radiative cooling was included in the simulation. Relatively strong winds were assumed in these studies, but radiative effects may be expected to be more prominent in lighter winds. André and Mahrt (1981) pointed out that in a strongly turbulent boundary layer the potential temperature, θ, is a concave function of the height, while it is convex in radiatively dominated boundary layers. Estournel and Guedalia (1985) emphasised the difference between strong and weak winds.

The past few decades have witnessed continuing progress in the field of atmospheric radiation. In particular, the water vapour continuum is now much better understood (Clough et al. (1989)). Radiation schemes have benefited from evaluation in intercomparisons such as ICRCCM (Ellingson and Fouquart (1991)). Recently there has been a renewal of interest in the impact of radiation in the boundary layer (*e.g.* Savijärvi (2006)), Edwards (2009a), Edwards (2009b) and Steeneveld et al. (2010)).

Below, we shall examine three issues of radiation and turbulence in the SBL, beginning with an overview of the role of longwave radiation. Subsequent sections will be concerned with the interaction between radiation and turbulence in light winds and the deepening of the boundary layer through the morning transition, as represented in GABLS3.

2 An Overview of Radiation in the Stable Boundary Layer

The discussion here, focusing entirely on conditions under clear-skies, is abbreviated from Edwards (2009a), which contains more details.

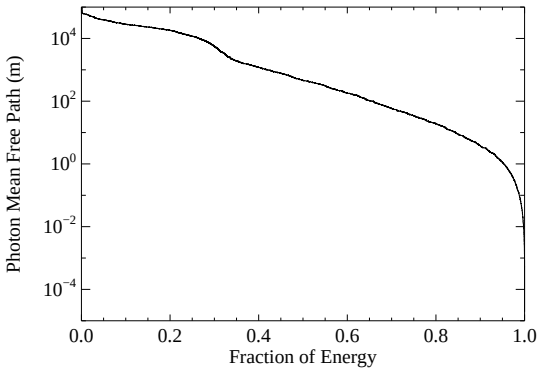

Figure 1: The photon mean free path for photons emitted from the surface into a radiative SBL.

Because the SBL is mainly a nocturnal phenomenon and LW radiation is very sensitive to the profile of atmospheric temperature, it is principally LW radiation that is of interest in the SBL. LW interactions in the atmosphere can be divided into a background cooling to space, a direct exchange with the surface and internal exchanges within the atmosphere. Cooling to space is the dominant contribution in most of the atmosphere. The exchange with the surface is important in the lowest few metres of the atmosphere, especially when the surface cools rapidly. Internal exchanges are sensitive to the curvature of the temperature profile and to gradients in the moisture content. Atmospheric absorption and emission are due mainly to water vapour and carbon dioxide. This absorption varies both strongly and rapidly with frequency, so that radiation is a fundamentally non-local process. Absorption by water vapour is concentrated in the rotation band (wavelengths greater than 12μm) and in the vibration-rotation band (wavelengths less then 8μm), while absorption by carbon dioxide is most significant around 15μm. Between 8 and 12μm absorption is weak and is principally due to continuum absorption by water vapour.

To illustrate the non-local impact of radiation, figure 1 shows the photon mean free path calculated at a temperature of 274 K and a specific humidity of 0.004. The horizontal scale associates the mean free path with the fraction of emitted energy in a Planckian distribution at this temperature. Only 5% of the photons emitted from the surface have mean free paths of less than 1m, while two thirds have mean free paths greater than 100m. In drier atmospheres the mean free paths will be longer, so the net LW flux at the surface is influenced by the temperature and moisture profiles through a significant depth of the atmosphere.

2.1 A Note on "Runaway" Cooling

There is sometimes a perception that the net LW flux at the surface is relatively insensitive to changes in surface temperature and it has consequently received less attention than the sensible heat flux in studies of the SBL. Although the radiative flux from the surface declines as the surface temperature falls, the associated cooling of air near the surface reduces the downward LW flux, so that the change in the net flux is smaller than the change in the upward flux. As mentioned before, in early work (*e.g.* Brunt (1941)) simple empirical formulae for the downward flux, of the form $LW^{\downarrow} = \sigma T_{2m}^4 \mathrm{fnc}(e_{2m})$, were used. It is then argued that since the relative changes in T_{2m} during the night are not large, neither the downward nor net LW flux changes significantly. However, such relationships are derived by statistical analysis of data for a large range of conditions and are based on the implicit assumption that the near-surface temperature and humidity are representative of the depth of the atmosphere which is in radiative contact with the surface. As just discussed, this depth can be significant, especially in the very dry conditions typical of the SBL in polar night. Under these conditions strong surface inversions may be encountered

and the assumption becomes invalid. Niemelä et al. (2001) have shown that, under such conditions, simple formulae of this type substantially underestimate the downward flux at the surface by as much as $60\mathrm{Wm}^{-2}$. Thus, whilst the surface temperature may indeed fall sharply in response to a sudden increase in net surface cooling, such as would result from a removal of cloud cover, the development of a strong inversion at the surface would rapidly reduce the net radiative flux to 0, preventing further significant reductions in the surface temperature. Indeed, calculations show that this process occurs on a timescale of a few hours. In practice, both the sensible and ground heat fluxes must be incorporated into the surface flux balance, but radiation plays a key role in such conditions, and a balanced assessment of all components of the flux budget is required.

3 The Evening Transition in Light Winds

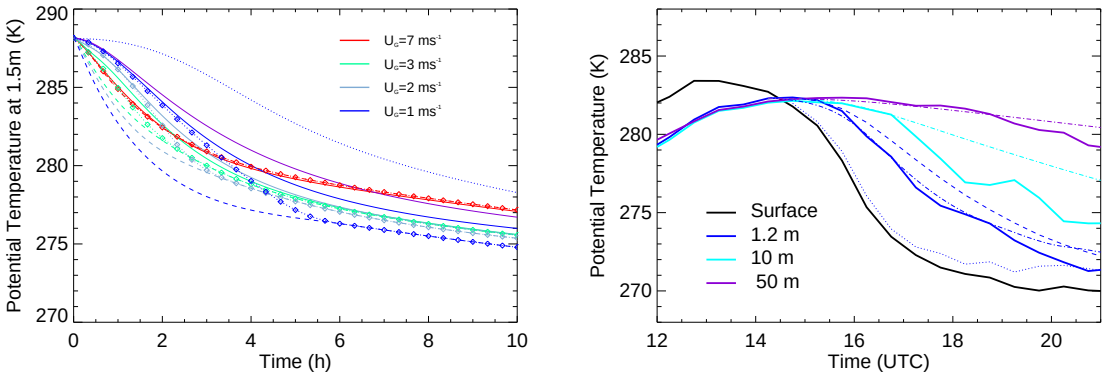

Figure 2: Left: The evolution of the potential temperature at 1.5m for the cooling of an initially neutrally stratified boundary layer at a potential temperature of 288.15K for a range of geostrophic wind speeds, as calculated in a highly resolved column model (solid lines, with wind speed indicated by colours), together with the predictions of surface similarity, shown as coloured dashed lines, and the prediction of the transitional diagnostic of near-surface air temperature, shown by broken lines with symbols. The solid purple line shows the evolution of the potential temperature in completely still conditions, while the dotted blue line shows the evolution for a wind-speed of $1\mathrm{ms}^{-1}$ for a simulation in which radiative cooling within the atmosphere is neglected, but the surface skin temperature is imposed from the simulation with a geostrophic wind speed of $1\mathrm{ms}^{-1}$ that included radiative cooling in the atmosphere. Right: The surface temperature (solid black line) and potential temperatures at 1.2, 10 and 50 m (solid coloured lines) observed at Cardington on 3 February 2007. Dot-dashed lines show the simulated potential temperatures from the highly resolved column model including radiative cooling in the atmosphere, while the dotted blue line shows the potential temperature at 1.2m calculated from the observations at 10m and at the surface using surface similarity theory. The dashed blue line shows the potential temperature at 1.2m, calculated for direct radiative cooling to the surface alone.

Although winters in north-western Europe are dominated by windy and cloudy conditions, more rarely anticyclonic conditions with clear skies and very light winds prevail. Under such conditions forecast near-surface air temperatures fall very rapidly through the evening transition while the observed temperatures may fall more slowly, so that forecasts may be subject to large cold errors.

Forecast near-surface air temperatures, at 1.5–2m, are predicted by applying surface similarity theory to interpolate between the surface skin temperature and the temperature on the lowest atmospheric grid-level of the model, typically at a height of 10m or more. In applying surface similarity theory, it is assumed that the fluxes of heat and momentum do not change significantly from their values at the surface up to the lowest grid level, so that the local Obukhov length, $\Lambda(z)$, remains essentially constant

and equal to its value at the surface. In a developed quasi-equilibrium SBL, the magnitudes of the fluxes will decrease linearly with height, so it might be thought that accounting for this variation would lead to significantly more accurate forecasts of near-surface air temperature. In fact, Delage (1997) showed that the decreases in Λ and the local turbulent temperature scale, θ_{*L}, largely cancel each other out, so that surface similarity performs rather well.

However, this argument is not applicable around the transition, when the heat flux will decrease more rapidly with height above the surface than the momentum flux. To investigate transitional conditions in more detail, a highly resolved one-dimensional model was constructed, based on local similarity and including radiation (Edwards (2009b). 30 levels are included below 1.5m, but there is no special treatment of the roughness sublayer. At the initial instant it is assumed that θ is constant in the boundary layer, while the wind speed has a logarithmic profile. At the surface, a time-varying skin temperature may be imposed, or a soil model may be included. For illustrative purposes, a simple force-restore scheme is used here.

Figure 2 shows the evolution of θ(1.5m) for imposed geostrophic wind speeds of 7, 3, 2, 1 and 0ms^{-1} for cooling from an initial profile with $\theta = 288.15$K as thick solid lines, with colours indicating the wind speed. The applicability of surface similarity theory to the diagnosis of near-surface air temperatures is examined by calculating θ(1.5m) from the wind speed at 10m and the difference in potential temperature between the surface and 20m, using surface similarity theory. These levels correspond to those used in the global forecasting configuration at the UK Met Office and are representative of the levels used generally in operational models. The potential temperatures thus calculated are shown as dashed lines. For a gesostrophic wind of 7ms^{-1}, shown in red, the potential temperature derived from surface similarity agrees closely with the actual value. For lower wind speeds, the actual potential temperatures in the first few hours after the transition are warmer than for higher wind speeds, while the opposite trend is seen in the values calculated from surface similarity theory. These values therefore show cold biases during the transition of 1–2K at 3 ms^{-1} and of more than 5K at 1ms^{-1}. At low winds speeds, surface similarity yields values which are too close to the surface temperature. To assess the contribution of atmospheric radiative cooling, the dotted blue line shows θ(1.5m) for a simulation where the surface temperature from the simulation with a wind of 1ms^{-1} and the force-restore surface scheme is imposed, but atmospheric radiative cooling is ignored. In the first few hours of the simulation, the reduction of θ(1.5m) is largely due to radiation. For comparison, the purple line shows θ(1.5m) for a simulation of completely still conditions with no turbulence.

Field observations taken at Cardington on 3rd February 2007 support this picture. On this day, skies were clear and the wind speed at 10m was about 1ms^{-1} until 19UTC, after which it increased. The black line in figure 2 shows the observed surface temperature, while the solid blue, cyan and purple lines show the observed potential temperatures at 1.2, 10 and 50m. The boundary layer was well-mixed until 14:30, whereafter it became stable and the surface cooled rapidly. Using the column model, a simulation was performed, starting from the observed profile of θ at the transition with an imposed wind of 1ms^{-1}, while the surface temperature was prescribed from the observations. The simulated potential temperatures are shown as dot-dashed lines, which agree very closely with the observed value through the early evening, except at 10m, where they diverge about 2 hours into the simulation. The dotted line shows the potential temperature calculated from the surface temperature, θ(10m) and the wind at 10m by applying surface similarity theory. As in the idealized model, this is evidently tied too closely to the surface temperature. The dashed blue line shows the potential temperature obtained if only radiative cooling directly to the surface is considered, while exchanges within the atmosphere are ignored, showing that cooling to the surface is the dominant contribution here.

3.1 Diagnosing Near-Surface Air Temperatures in Light Winds

It is clearly not feasible to use such high vertical resolution in a GCM, so a parametrization is now sought. The parametrization must include the effects of radiative cooling in light winds, must coincide with standard theory in strong winds, and must be expressed in terms of quantities readily calculated in a GCM. Initial experiments, based on the instantaneous bulk Richardson number of the lowest model layer, showed some amelioration of cold biases following the evening transition; but the diagnosis of warmer temperatures at 1.5m later in the night reduced the magnitude of the warming increments applied during data assimilation, producing a detrimental cooling in the following forecast. A more elaborate scheme has therefore been developed, targeted at the transition, with the tendency to decoupling suppressed thereafter.

As shown above, radiative cooling is dominated by that directly to the surface, which may be represented as $-\dot{T}_{\rm rad}(z) = \mathscr{K}(T(z) - T(0))$, where $\mathscr{K}$ depends on the height z and the concentration of water vapour and carbon dioxide.

To develop a representation of the effects of turbulence, it is helpful to return to the highly resolved model, but to consider a simpler situation, in which a constant surface cooling rate is imposed and atmospheric radiative cooling is ignored. Under these conditions, the development of the SBL after the transition may conceptually be divided into two phases: a rapid initial phase, in which turbulence in the surface layer decays, and a subsequent slower phase, in which rotational shear caused by the Coriolis force reinvigorates the turbulence. The first phase must depend on the relative importance of the surface cooling rate, $\dot{\theta}_0$, and the wind speed, which we shall characterise with the initial surface friction velocity, u_{*0}. On dimensional grounds we then obtain scales for the time, length and temperature:

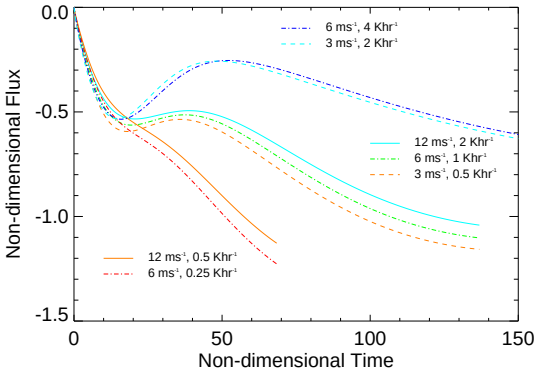

Figure 3: The non-dimensional sensible heat flux at the surface plotted against the non-dimensional time for a range of surface cooling rates and wind speeds.

$$\mathscr{T} = \sqrt{\left(\frac{u_{*0}}{\frac{g}{\theta_{00}}\dot{\theta}_0}\right)}, \qquad \mathscr{L} = \sqrt{\left(\frac{u_{*0}^3}{\frac{g}{\theta_{00}}\dot{\theta}_0}\right)}, \qquad \text{and} \qquad \Theta = \dot{\theta}_0\sqrt{\left(\frac{u_{*0}}{\frac{g}{\theta_{00}}\dot{\theta}_0}\right)}. \tag{1}$$

An alternative conceptual argument can be made by noting that the time for the cooling at the surface to be experienced at a height, z, will be $O(z/u_{*0})$, in which time the surface will have cooled by $\dot{\theta}_0.z/u_{*0}$, so we obtain a Richardson number

$$Ri = \frac{\frac{g}{\theta_0}\dot{\theta}_s\frac{z}{u_{*0}}.z}{u_{*0}^2} = \left(\frac{z}{\mathscr{L}}\right)^2. \tag{2}$$

Essentially, $\mathscr{L}$ is the depth of the atmosphere which responds to the cooling at the surface.

Figure 3 shows the non-dimensional surface heat flux plotted against the non-dimensional time for simulations with different wind-speeds and cooling rates. The fluxes largely collapse according to these scalings. With strong winds and slow surface cooling the heat fluxes continuously increase in magnitude; but with weak winds and rapid surface cooling the heat flux first increases in magnitude and then decreases, before increasing once more, but at a slower rate. This slower growth is associated with a

re-invigoration of turbulence caused by directional shear at the top of the surface layer and occurs on the Coriolis timescale, f^{-1}. Thus, the effectiveness of strong cooling at the surface in stabilizing the surface layer and tending towards a decoupled state may be measured by the ratio of these timescales:

$$\mathscr{D} = \sqrt{\frac{(g/\theta_{00})\dot{\theta}_0}{u_{*0}f^2}}. \tag{3}$$

In the parametrization, the diagnosis of $\theta(z_s)$ (z_s being the height at which the near-surface air temperature is diagnosed) is unaltered in unstable conditions, being based purely on similarity theory; but if a transition to stable conditions is diagnosed the evolution of $\theta(z_s)$ is explicitly considered. The time since the transition is stored and at each timestep $\theta(z_s)$ is adjusted for radiative cooling to give a provisional radiative value, $\theta_{\rm rad}(z_s)$. A further provisional diagnosis of $\theta(1.5\text{m})$, $\theta_{\rm sim}(z_s)$, is made using standard surface similarity theory and $\theta(z_s)$ is interpolated between these two values as $W\theta_{\rm rad} + (1-W)\theta_{\rm sim}$, where W is a function of the timestep, δt, $z_s/\mathscr{L}$ and u_*/z_s. Whilst this parametrization is largely heuristic, it does incorporate the ideas that the times for the evolution to affect the air temperature will be $O(z/u_*)$ and that $\mathscr{L}$ is the depth of the atmosphere that cools with the surface. Here, u_* and $\mathscr{L}$ are taken as instantaneous values, rather than those exactly at the transition to allow for changing meteorological conditions. Also, u_* must be diagnosed from surface similarity and so is an underestimate of the value which would have been obtained from a highly resolved simulation: this is accounted for in tuning the scheme.

The curves in figure 2 marked with diamonds show the results of applying this parametrization to the idealized simulations and setting

$$W = \exp(-0.4f\delta t).\frac{1}{1+\min\left(0.000283\delta t\left\{\frac{\mathscr{L}}{z_s}\log\left(1+\frac{z_s}{z_0}\right)\right\}^2,\ \frac{0.2u_*\delta t}{z_s}\right)}. \tag{4}$$

For winds of 1 and 2ms^{-1} it represents the temperature shortly after the transition quite well, but intentionally collapses towards the value obtained from similarity theory a few hours later. For a wind of 3ms^{-1}, the degree of decoupling is less and is underestimated by the parametrization.

To illustrate its impact on a forecast, we consider 17 February 2008, when a large anticyclone lay over Europe and skies were clear and winds light over England and the Low Countries. Figure 4(top) shows the synoptic chart at 18UTC on this day, while the lower panels show the composite MODIS image shortly after noon on the day, the observed wind speeds at synoptic stations at 17UTC and the corresponding predicted winds at the same sites, taken from the forecast initialized at 12UTC on the day. Qualitatively, there is good agreement between the observed and forecast winds, although the area of very light winds (about 1ms^{-1}) is underestimated. Figure 5 shows the impact of this transitional diagnostic on the forecast temperatures at 1.5m at 17UTC and the errors relative to synoptic observations without the diagnostic (central panel) and when it is included (right panel). Without the transitional diagnostic, significant cold biases are observed in regions of light winds (less than 2ms^{-1}), while these biases are reduced when it is included. Comparison of the forecast surface temperature with retrieved values (not shown) indicates that the difference between the surface and 1.5m temperatures is more accurately forecast with the transitional diagnostic.

3.2 Further Comments

Although the transitional diagnostic performs well in cases such as this, a number of issues require further investigation. The relative importance of turbulent and radiative effects has been represented on the basis of local scaling and no detailed model of the roughness sub-layer has been included: both these issues could modify the approach to the radiative limit. Moreover, the column model has been initialized

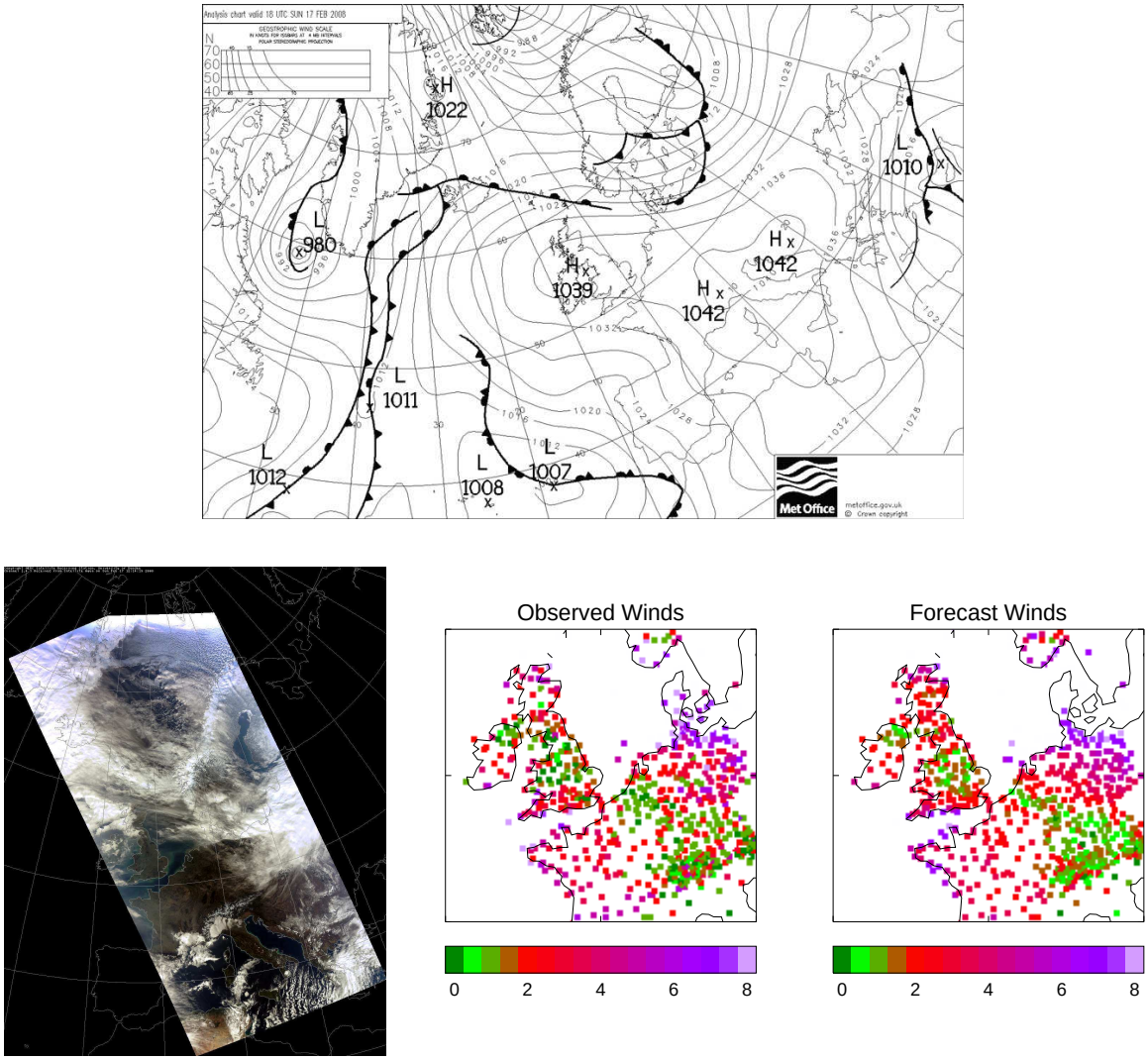

Figure 4: Top. The analysed surface pressure at 18UTC on 17 February 2008. Lower left. The composite MODIS image at 12.14 on the same day. (Image obtained from the NERC satellite receiving station, Dundee University, Scotland.) Lower centre. The observed 10m wind speed at synoptic stations at 17UTC on 17 February 2008. Lower right. The forecast 10 m wind speeds at the same locations.

with a unidirectional logarithmic wind profile and a uniform potential temperature in the boundary layer. It may be asked whether this is a realistic representation of the profiles at the transition and what role decaying convective turbulence might play. Large-eddy simulation can in principle help to resolve these issues. However, very high resolution is required to model such cases and the performance of sub-grid models in very light winds may be questionable. Preliminary large-eddy simulations suggest that even with fairly weak surface heating during the day, well-mixed profiles of wind and potential temperature are established during the day, so that directional wind shear in the boundary layer at the transition is small, while θ is essentially uniform. Imposing a rapid rate of surface cooling (while ignoring atmospheric radiative cooling) produces a state where the upper part of the developing SBL remains close to neutrality, while larger Richardson numbers are encountered near the surface: this may indicate that under very rapid cooling the surface layer becomes so stable that decaying convective turbulence cannot penetrate into it; however, further work is required.

The diagnostic does not take any account of intermittency or of gravity currents. Gravity currents are

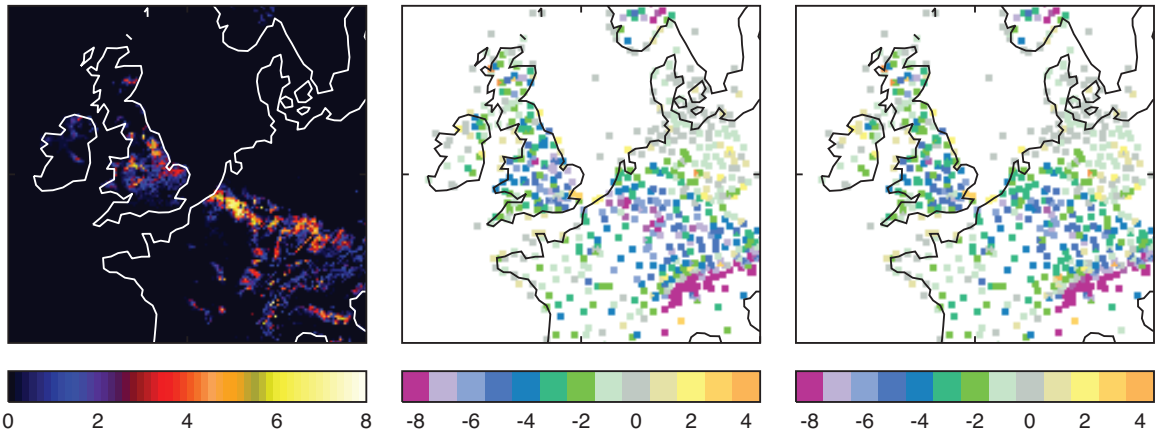

Figure 5: Left. The impact of the transitional near-surface air temperature diagnostic at 17UTC on 17 February 2008. Centre. The errors in near-surface air temperature in the control forecast at synoptic stations at 17UTC, Centre. The errors in near-surface air temperature with the transitional near-surface air temperature diagnostic.

very likely to form after the transition, but the timescale will depend on the slope, which raises the possibility that the SBL shortly after the transition may be more predictable than that later in the night. Strongly radiatively dominated boundary layers are relatively rare and may easily be disrupted by intermittent turbulence. Indeed, the potential temperature at 10m in the example from Cardington shown above may exemplify such a phenomenon. Conversely, further examination of data from Cardington (Edwards et al. (2011)) suggests that surface similarity still tends to tie the near-surface and surface temperatures too closely later in the night, so some representation of nocturnal decoupling should ultimately be included in forecasting models.

4 Radiative Deepening of the Boundary Layer at the Morning Transition

Garratt and Brost (1981) and Tjemkes and Duynkerke (1989) have shown that radiative exchanges between the residual layer and the underlying nocturnal boundary layer (NBL) increase the stability of the residual layer, but reduce that of the NBL, causing the NBL to be about 20% deeper by the end of the night than in simulations where radiation is neglected. The influence of radiation on the ensuing morning transition was not examined in these studies, but this may conveniently be done using the large-eddy case of GABLS3.

The large-eddy case of GABLS3 is initialized with a prescribed atmospheric profile at 00UTC and extends through the morning transition to 09UTC. The sensible heat flux at the surface becomes positive just after 05UTC and the morning transition begins. In the standard version of the case radiation is omitted, but additional simulations including radiation have been carried out with the large-eddy model of the UK Met Office. Figure 6 shows profiles of θ at hourly intervals between 05 and 09UTC from simulations with and without radiation. Green lines show profiles for the standard case, blue lines profiles including LW radiation and red lines profiles including both LW and SW radiation. At 05UTC, the NBL is slightly deeper when radiation is included, but since the simulations have been initialized with the same profile of θ at 00UTC, the full impact of radiation on the NBL is not seen. Thereafter, the simulations which include radiation show more rapid deepening of the boundary layer, particularly between 08 and 09UTC, when the developing mixed layer finally grows through the top of the NBL. This deepening of the mixed layer improves agreement with measurements of θ made from the tower.

The lower boundary condition in GABLS3 consists of a prescription of θ at 0.25m, which effectively

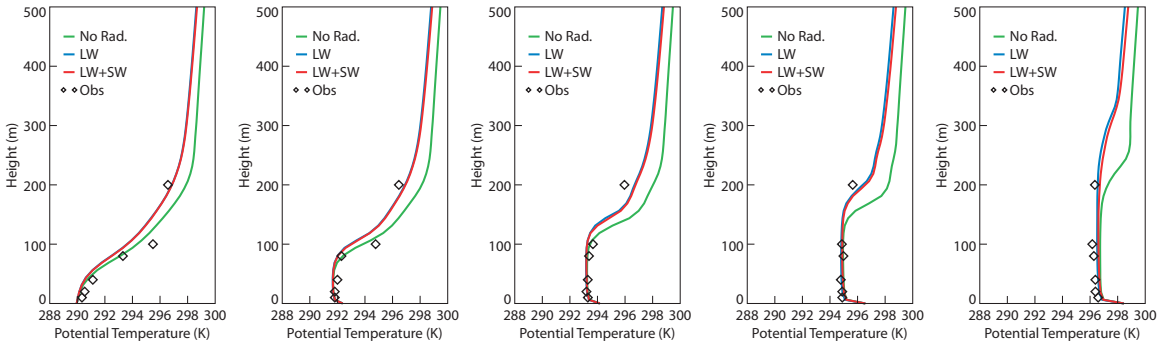

Figure 6: Profiles of the potential temperature at hourly intervals from 05UTC to 09UTC for the GABLS3 large-eddy case, showing simulations without radiation, with LW radiation alone and with both LW and SW radiation. Observed values at 10, 20, 40, 80, 100 and 200m are also shown.

constrains the temperature of the mixed layer. LW radiative cooling of the residual layer therefore reduces the stability of the capping inversion, leading to increased entrainment and faster growth of the mixed layer. Moreover, LW cooling is strongest around 200m, the top of the NBL, so that the reduction in the strength of the capping inversion is most pronounced here and the increase in the rate of growth of the mixed layer is greatest. Absorption of SW radiation in the atmosphere has only a small effect, with the resulting warming slightly stabilizing the profile and reducing the rate of growth of the mixed layer.

5 Summary and Conclusions

A good understanding of the surface flux budget, both in models and observations, is an essential prerequisite for the successful representation of the SBL in forecasting and climate models. This understanding must encompass both the radiative and ground heat fluxes in conjunction with the turbulent fluxes. The non-local nature of radiation has been emphasised to stress the importance of the downward radiative flux in polar night.

In addition to its role in the surface flux budget, atmospheric radiative cooling in the SBL cannot be neglected. Radiative exchanges at the top of the SBL cause it to be deeper than it would be if there were no atmospheric radiative cooling; this deepening is especially pronounced through the morning transition. It is therefore desirable that radiation should be included in large-eddy simulations of the stable boundary layer

In light winds, radiative cooling near the surface can be the dominant factor in determining near-surface air temperatures after the evening transition. The inclusion of radiative and transient effects in the diagnosis of near-surface air temperatures following the transition can yield significant improvements in forecasting accuracy under these conditions, but greater theoretical understanding of this régime is needed.

References

André, J. C. and L. Mahrt, 1981: The nocturnal surface inversion and influence of clear-air radiative cooling. *J. Atmos. Sci.*, **39**, 864–878.

Brunt, D., 1941: *Physical and Dynamical Meteorology*. Cambridge University Press, 428 pp.

Clough, S. A., F. X. Kneizys, and R. W. Davies, 1989: Line shape and the water vapor continuum. *Atmos. Res.*, **23**, 229–241.

Cuxart, J., A. A. M. Holtslag, R. J. Beare, E. Bazile, A. Beljaars, A. Cheng, L. Conangla, M. Ek, F. Freedman, R. Hamdi, A. Kerstein, H. Kitagawa, G. Lenderink, D. Lewellen, J. Mailhot, T. Mauritsen, V. Perov, G. Schayes, G.-J. Steeneveld, G. Svensson, P. Taylor, W. Weng, S. Wunsch, and K.-M. Xu, 2006: Single-column model intercomparison for a stably stratified atmospheric boundary layer. *Boundary-Layer Meteorol.*, **118**, 273–303.

Delage, Y., 1997: Parameterising sub-grid vertical transport in atmospheric models under statically stable conditions. *Boundary-Layer Meteorol.*, **82**, 23–48.

Edwards, J. M., 2009a: Radiative processes in the stable boundary layer: Part I. radiative aspects. *Boundary-Layer Meteorol.*, **131**, 105–126, doi:10.1007/s10546–009–9364–8.

— 2009b: Radiative processes in the stable boundary layer: Part II. the development of the nocturnal boundary layer. *Boundary-Layer Meteorol.*, **131**, 127–146, doi:10.1007/s10546–009–9363–9.

Edwards, J. M., J. R. McGregor, M. R. Bush, and F. J. Bornemann, 2011: Assessment of numerical weather forecasts against observations from cardington: seasonal diurnal cycles of screen-level and surface temperatures and surface fluxes. *Q. J. Royal Meteorol. Soc.*, **137**, 656–672.

Ellingson, R. G. and Y. Fouquart, 1991: The intercomparison of radiation codes in climate models: An overview. *J. Geophys. Res.*, **96**, 8,925–8,927.

Estournel, C. and D. Guedalia, 1985: Inflence of geostrophic wind on atmospheric nocturnal cooling. *J. Atmos. Sci.*, **42**, 2695–2698.

Funk, J. P., 1960: Measured radiative flux divergence near the ground at night. *Quart. J. Royal Meteorol. Soc.*, **86**, 382–389.

Garratt, J. R. and R. A. Brost, 1981: Radiative cooling rates within and above the nocturnal boundary layer. *J. Atmos. Sci.*, **38**, 2730–2746.

Niemelä, S., P. Räisänen, and H. Savijärvi, 2001: Comparisons of surface radiative flux parameterizations Part I: Longwave radiation. *Atmos. Res.*, **58**, 1–18.

Savijärvi, H., 2006: Radiative and turbulent heating rates in the clear-air boundary layer. *Quart. J. Royal Meteorol. Soc.*, **132**, 147–161.

Steeneveld, G. J., M. J. J. Wokke, C. D. G. Zwaaftink, S. Pijlman, B. G. Heuskinveld, A. F. G. Jacobs, and A. A. M. Holtslag, 2010: Observations of the radiation divergence in the surface layer and its implication for its parameterization in numerical weather prediction models. *J. Geophys. Res.*, **115**, doi:1029/2009JD013074.

Tjemkes, S. A. and P. G. Duynkerke, 1989: The nocturnal boundary layer: Model calculations compared with observations. *J. Appl. Meteorol.*, **28**, 161–175.